AMERICAN SCIENTIFIC PUBLISHERS

Journal of Medical Imaging and Health Informatics
Vol. 5, 1208–1216, 2015

A Method for Liver Segmentation on Computed Tomography Images in Venous Phase Suitable for Real Environments

Fernando López-Mir[1,*], Pablo González[1], Valery Naranjo[1], Eugenia Pareja[2], Sandra Morales[1], and Jaime Solaz-Minguez[3]

[1]*Instituto Interuniversitario de Investigación en Bioingeniería y Tecnología Orientada al Ser Humano, I3BH/LabHuman, Universitat Politècnica de València, Camino de Vera s/n, 46022 Valencia, Spain*
[2]*Unidad de Cirugía Hepatobiliopancreática y Trasplante, Hospital Universitari i Politècnic La Fe, Av. Fernando Abril Martorell 106, 46026 Valencia, Spain*
[3]*Hospital Clínica Benidorm, Av. de Alfonso Puchades 8, 03501 Benidorm, Alicante, Spain*

Nowadays, different methods are being published for the segmentation of the liver but, in general, most of them are not suitable for clinical practice due to several inconveniences as high computational cost, excessive user dependence or low accuracy. The purpose of this paper is to present the performance and validation of a liver segmentation method in computed tomography images (contrast venous phase) where automation, easy user interaction, and low computational cost (besides the required accuracy for clinical purposes) have been taken into account. Firstly, an adaptive filter based on intrinsic parameters of the liver is applied to reduce noise but preserving external liver gradients. In a second step, from a seed or a group of them, voxels with similar intensities are included in an initial 3D mask. Finally, thanks to the combination of morphological operators in different orientations, several non-liver structures (cava vein, ribs, stomach or heart) are removed and the final 3D liver mask is obtained. Thirty public datasets have been used to estimate the accuracy of the proposed algorithm, twenty for training the method and ten for testing it. An average Jaccard index of 0.91 (±0.03), a Hausdorff distance of 26.68 (±10.42) mm, and a runtime of 0.25 seconds per slice, state a promising efficiency and efficacy in the test datasets. To our knowledge, liver segmentation methods in the state of the art are achieving high accuracy at the expense of requiring an exhaustive training stage and so much clinician interaction time in different steps of the process. In this paper, a method based on intensity properties is carried out with a high grade of automatism, an easy user interaction and a low computational cost. The results obtained for different patients state a low variance and a good accuracy in most images, thus the robustness of the method is demonstrated.

Keywords: Liver Segmentation, Intensity Model Algorithm, Mathematical Morphology, Hepatic Planning, Computer Tomography.

1. INTRODUCTION

Hepatocellular carcinoma is the responsible of most liver cancers, the sixth most common cancer in the world, the main reason of death in cirrhotic people and it is also the third cause of death by neoplasm. Besides, other types of liver cancers as Fibrolamellar carcinomas, liver metastases, hepatoblastomas or angiosarcomas show the social impact of this disease. Nowadays, hepatic tissue anomalies are treated with a qualitative comparison of computed tomography (CT) or magnetic resonance images (MRI) thanks to physician experience; however, quantitative measures are not extended. Liver segmentation is the first step to help surgeons or radiologists to delimit lesions in this organ, and thus liver/lesions ratios and measures could be calculated. An accurate liver segmentation has a direct application in planning, monitoring, and treatment of different types of pathologies such as cirrhosis or hepatocellular carcinoma diseases[1] or in liver transplant surgery, but liver segmentation in CT images is currently an unsolved problem.[2–4] To author's concern, there is not a software for liver surgery planning in clinical practice. The first limitation for that is the necessity of a reliable and widely validated method of liver segmentation. This requirement is essential to be able to apply this kind of software in clinical practice.

Liver segmentation algorithms are applied to MRI or CT images. In the literature, these methods are more commonly used in CT[1–18] than in MRI[4,19] for different reasons: CT has a better gradient response than MRI, it has less artefact effects because

*Author to whom correspondence should be addressed.

 2156-7018/2015/5/1208/009 doi:10.1166/jmihi.2015.1509

the movement is less (a CT study requires an acquisition time of 2–3 minutes whereas a MR analysis requires 6–8 minutes) and, consequently, CT involves less cost than MR. Currently, some efforts are being focused on the liver segmentation in other image modalities as positron emission tomography (PET) or ultrasounds but the poor spatial resolution is a crucial disadvantage that neither manual corrections can solve in some cases for clinician purposes.[20–22]

Liver segmentation methods can be classified according to several criteria: user interaction, input image type, algorithm properties, etc. Regarding the algorithm properties, the methods can be divided in greylevel-based and contour-based methods. Contour-based methods generally achieve better results in liver segmentation but a more complex interaction, initialization, and/or training process is required in order to obtain the desired results. These characteristics can be inappropriate in a clinical environment. Probabilistic atlases, level-sets, deformable models, statistical shape models are algorithms used in liver segmentation which are based on contour properties.[1–14] Probabilistic atlases require a manual segmentation of several livers in order to form the atlases.[5,6] This part requires a hard work, since the robustness of the method is related to the quality of manual liver segmentations that forms the atlas. Then, a registration algorithm is performed to find out the correspondence between the liver atlas and this structure in the new image. The computational cost of this process can be higher than 30 minutes in some cases.[5] Level set algorithms fit an initial curve to the boundary of the organ of interest, in our case the liver. These algorithms also need training[7] or an initial iteration to form the initial curve, for example with more than 30 seeds[8] or drawing this initial curve.[10] Some efforts are focused on providing this initial curve in an automatic way but the accuracy of the algorithm decreases[11] or computational cost increases more than 10 minutes for a typical dataset of 100–120 slices.[9] In the case of statistical or deformable models, a hard training is also required in a similar way to the probabilistic atlases.[13,14] Additionally, the computational cost increases considerably in these methods and therefore the clinical usability decreases. For those reasons (computational cost, training, and hard user interaction) these algorithms can be accurate but their clinical application is limited.

Greylevel-based methods have a lower computational cost but these algorithms are less robust to noise and gradient changes. Thresholding algorithms, classifiers as k-means, or region growing methods belong to this group of algorithms.[16–19] Region growing methods need some seed points in order to use some greylevel criteria for pixel addition to the liver mask.[16,17,19] Thresholding algorithms use histogram properties to classify pixels, thus these methods are optimized for a determined type of images with similar histograms properties.[18] These methods can obtain promising results and thanks to the reasonable computational cost and the low training required, they could be optimal for clinical environments.[16,19] Efficient pre- and/or post-processing steps are needed in order to reduce noise and adjacent organs connections in this kind of algorithms to carry out an accurate segmentation but these processes could increase the computational cost and the user interaction and similar problems to contour-based methods may appear.[19]

User iteration increases the method accuracy but it reduces their usability due to the consuming of clinician's time and the final algorithm can obtain user-dependent results.[2,7,8] So, it is important to balance the user interaction and the automation of the method (the behaviour of greylevel methods are better in these issues) and the robustness and accuracy of the final segmentation (the behaviour of contour-based methods are better in these cases).

The primary contribution of this paper is the design and validation of some pre- and post-processing steps in order to perform a 3D region growing algorithm for the segmentation of the liver in CT venous phase images. Region growing algorithm has the advantages of a low computational cost and no training requirements. These conditions are combined, in the proposed work, with an easy user interaction, and a considerable robustness and accuracy, provided thanks to the pre- and post-processing filters designed. The selection of this algorithm is based initially on the accurate results of some authors.[16,19] However, the main problems of these algorithms are the pre- or post-processing steps used, that increase the computational cost and therefore, clinical utility is reduced. Besides the selection of an optimum criterion that allows an accurate 3D growing, the success of our proposal lies in the design of these pre and post processing stages which turn a 3D region growing algorithm into a suitable solution for clinical use, i.e., a reasonable balance between accuracy, robustness, computational cost, and user interaction.

The liver segmentation method proposed in this paper is included within the framework of the HepaPlan project.[23] The aim of HepaPlan is the development of a planning system for hepatic surgery, Figure 1, which is currently under clinical validation.

After the liver tissue extraction, internal structures (hepatic veins and arteries, or biliary ducts) and lesions will be segmented. These segmented structures are obtained from different studies of the same patient, and, therefore, a registration step is required to have this information in a common 3D space. The correct segmentation and registration of these hepatic structures is needed in order to develop several tools for surgeons and radiologists: to compute different measures (such as tumour volume or area) or ratios (liver/tumour volume); to calculate distance between lesions and other structures; to obtain tumour position in Couinaud classification; and to carry out virtual resections for hepatic transplants.

The rest of the paper is divided into three sections. Section 2 reminds some tools used in our algorithm and explains the developed algorithm. Section 3 presents the final results and Section 4 states a discussion of our conclusions and outlines the future work.

2. METHOD

2.1. Theoretical Background

Region growing methods are based on neighbourhood greylevel intensities to expand an initial seed (or group of seeds) to obtain a final mask of the region of interest. With this initial seed (or seeds), a pixel is added to the mask (in our case the liver mask) if it fulfils two conditions: it is connected to the pixels that have already been labelled as liver and it satisfies some similitude criterion (different similitude criteria define different region growing algorithms). In our work, this criterion is defined as

$$f(x) \in m_0 \pm k * \sigma_0 \quad (1)$$

where $f(x)$ is the intensity of a new candidate pixel with coordinates $(x = (x, y))$, m_0 and σ_0 are the average and the standard

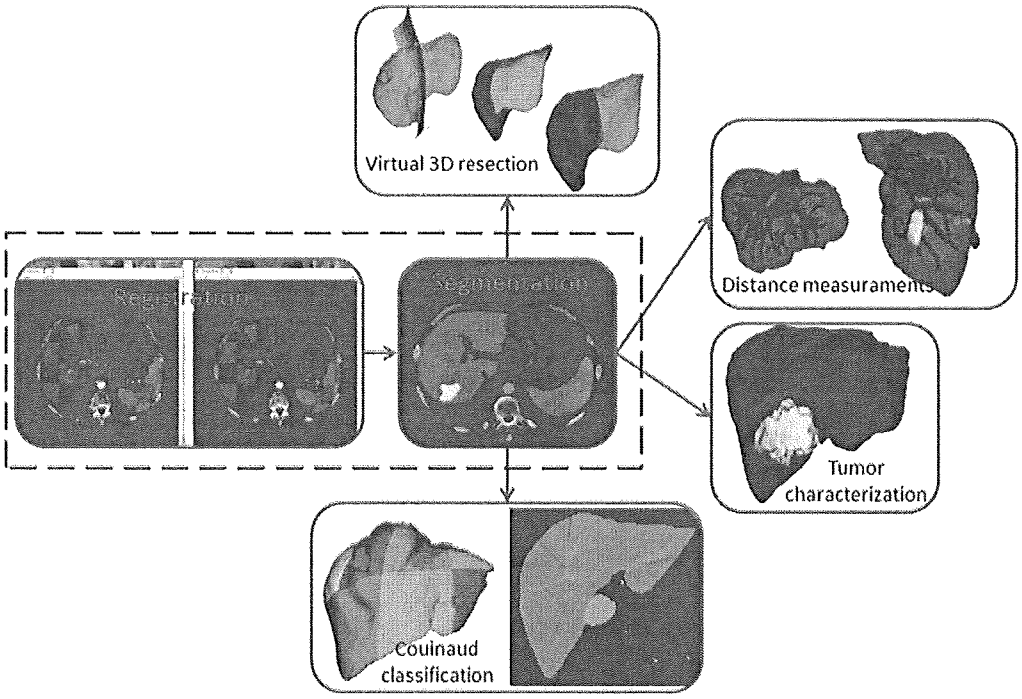

Fig. 1. HepaPlan project framework.

deviation of the pixel values of an initial liver mask and k is a tolerance parameter. This formulation is extensive to 3D volumes, only the connexion criteria between voxels changes. If the algorithm begins with a seed point (and not with an initial mask), m_0 and σ_0 is calculated using a neighbourhood around this seed point.

Mathematical morphology is a non-linear processing technique in spatial structures that is based on maxima and minima operators.[25] Erosion and dilation are the two basic operators:

$$\begin{aligned} &\text{Dilation: } [\delta_B(f)](x) = \max_{b\in B(x)} f(x-b) \\ &\text{Erosion: } [\varepsilon_B(f)](x) = \min_{b\in B(x)} f(x+b) \end{aligned} \tag{2}$$

where $B(x)$ is the structuring element centred at point (x) with a particular size and shape and $f(x)\colon E \to T$ is a greyscale image where $x \in E$ is the pixel position and T represents the pixel greylevel.

Other filter based on mathematical morphology that is used in this paper is the reconstruction by dilation and the partial reconstruction by dilation.[26] The reconstruction by dilation of an image $g(x)$ from a marker image $f(x)$ is defined as a geodesic dilation of the image f with respect to other image g, called reference, up to idempotence:

$$R_g^{\delta}(f) = \delta_g^{(i)}(f) \tag{3}$$

where $\delta_g^{(i)}(f)$ is such that $\delta_g^{(i)}(f) = \delta_g^{(i+1)}(f)$, and where $\delta_g^{(i)}(f) = \delta_g^{(1)}(\delta_g^{(i-1)}(f))$ being $\delta_g^{(1)}(f) = \delta_B(f) \wedge g$ the geodesic dilation with the unitary structuring element (a disk of radius equal to one pixel).

The partial reconstruction by dilation instead of applying the geodesic dilation $(\delta_g^{(i)}(f))$ up to the idempotence, it is carried out N times, i.e., $i \in \square$, $i = 1, 2, \ldots, \square$.

The close-hole operator can be defined from the reconstruction by dilation. In greylevel images, any set of connected voxels surrounded by connected components of higher values than the surrounding is considered a hole. This operator fills all the holes in an image $f(x)$ that do not touch the marker image f_δ:

$$\psi^{ch}(f) = [R_{f^c}^{\delta}(f_\delta)]^c \tag{4}$$

where f^c is the complement image of f, and f_δ is the image border defined in 2D as:

$$f_\delta(x) = \begin{cases} 255, & x = 0 \| y = 0 \| x = \text{width} \| y = \text{height} \\ 0, & \text{otherwise} \end{cases} \tag{5}$$

2.2. Algorithm

The diagram block of our algorithm is presented in Figure 2. The first purpose of the algorithm is to obtain a CT volume with a liver tissue as uniform as possible but preserving the gradient between adjacent organs.

Several smoothing filters were evaluated: a curvature flow filter (CF),[27] a morphological centre filter (MC),[26] and the adaptive filter (AF) proposed in this paper that is based on first-order statistics of the image, such as the average of the greylevel values (m) and their standard deviation (σ). This filter changes the pixel intensity as:

$$f(x) = \begin{cases} m_5 & \text{if } m_5 \in m \pm \sigma \\ f(x) & \text{otherwise} \end{cases} \tag{6}$$

where m_5 is the average of the circular pixel neighbourhood of radius 5 and m and σ are an initial estimation of the average greylevel of the liver values and their standard deviation, respectively.

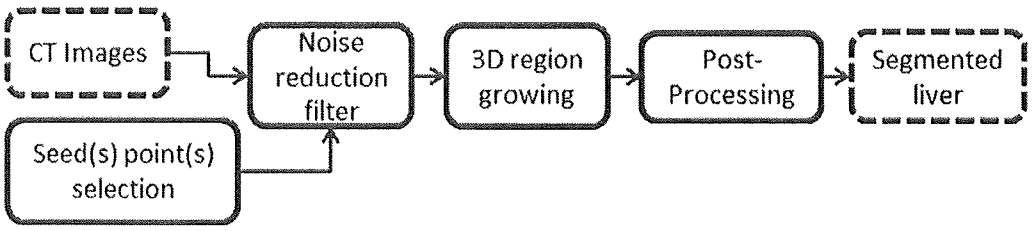

Fig. 2. Segmentation algorithm flowchart.

These parameters (m, σ) are calculated using a 2D region growing with a seed point selected by the user in one slice where the liver appears as large as possible and with homogeneous greylevel in the liver tissue (Fig. 3(a)). For this region growing 2D, the k parameter has been extracted experimentally ($k = 1.2$) and the m_0 and σ_0 parameters that control the region growing (Eq. (1)) are calculated in a circular neighbourhood of radius 25, centred in this selected seed. Each pixel in the final mask of this 2D region growing is considered for calculating the m and σ parameters needed by the adaptive filter. With these parameters, the adaptive filter is applied to the whole 3D study according to Eq. (6). Several experiments demonstrate that the adaptive filter obtains a more uniform grey-level in the liver reducing the noise and preserving better its boundaries than other approaches. Quantitative comparisons will be presented in Results section.

In the next step, a 3D region growing is applied to the smoothed CT volume (Figs. 3(b) and (c)), Eq. (1). The whole mask obtained as result of the previous 2D region growing is used as seed for the 3D region growing algorithm, so m_0 and σ_0 parameters are set to m and σ respectively (the adaptive filter parameters). The tolerance ($k = 1.85$) is extracted empirically using several datasets for evaluating the optimal tolerance parameter.

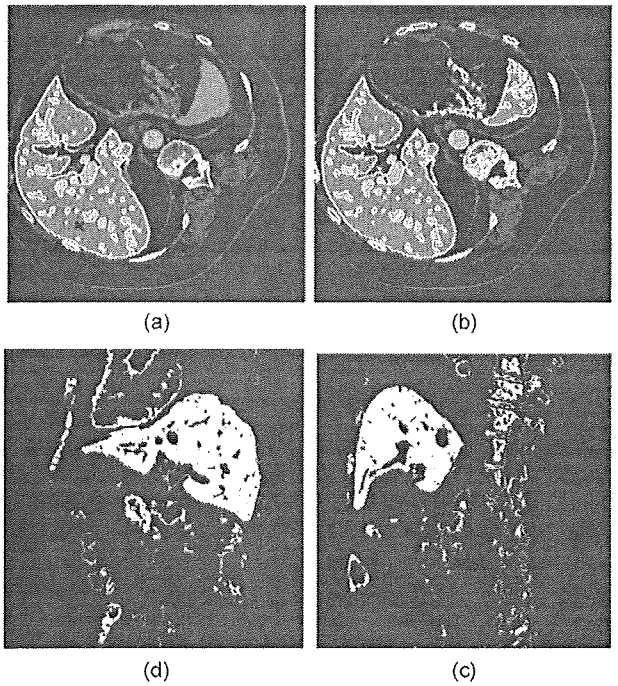

Fig. 3. (a) 2D region growing output (original slice and contour superimposed and seed in black cross position); (b) one slice of the 3D region growing (original slice and contour superimposed); (c) output 3D region growing masks in sagittal/coronal views.

At this point, the 3D liver mask states two problems. On one hand, an over-segmentation is produced by organs connected to the liver and with similar greylevel. It is the case of the ribs, cava/portal vein, heart and stomach. These connections appear frequently in all patients, but not always all structures are over-segmented as it depends on the type of study, the contrast agent and the anatomical patient's features. On the other hand, the method obtains the under-segmentation of some lesions with a greylevel lower than liver tissue.

Organ over-segmentation is solved with several post-processing filters focused on two main steps: an erosion to break connections between organs followed by a partial reconstruction to recover and refine the liver boundaries, as it is depicted in Figure 4.

The problem of the under-segmentation is solved with a close-hole operator. Only lesions in external zones of the liver tissue, the close-hole filter in axial view doesn't have effect because the lesion touches the liver border. Taking into account to the datasets used for the validation of the method, this situation is not common but to minimize this drawback the filter is applied in the three main views of the 3D study (axial, coronal and sagittal).

2.3. Post-Processing

Figure 4 shows the flowchart of the post-processing stage and Figure 5 depicts the results of the different steps. Firstly, 2D erosion is applied to the axial masks with a structuring element, $B_1(x)$ (Fig. 5(a)). In the eroded masks, M_E, the holes are closed using the close-hole operator in the three main directions of the eroded masks (axial, sagittal and coronal), the largest 3D object (the liver) is selected being 2D dilated in axial direction, with the same structuring element than the 2D erosion to try to recover the original size of the liver, obtaining the mask M_D (Fig. 5(b)). Erosion and dilation are not lineal operators, so it is not possible to recover completely the original size with this 2D dilation. For this reason, a partial reconstruction is performed under M_D using M_{CH} masks (where the contours are better defined) as marker images, to refine the resulting contour of the 2D dilation (Fig. 5(c)).

Finally, the mask contour is smoothed using Fourier descriptor filtering technique,[28] as previously proposed in Ref. [19], obtaining the final liver mask (Fig. 5(d)).

3. RESULTS

The goodness of our method has been evaluated with 30 public studies (sliver07 dataset), the same way that most authors follow to validate their algorithms.[2, 5, 8, 10, 13, 14, 16] A collection of 20 studies were provided with manual reference in order to tune

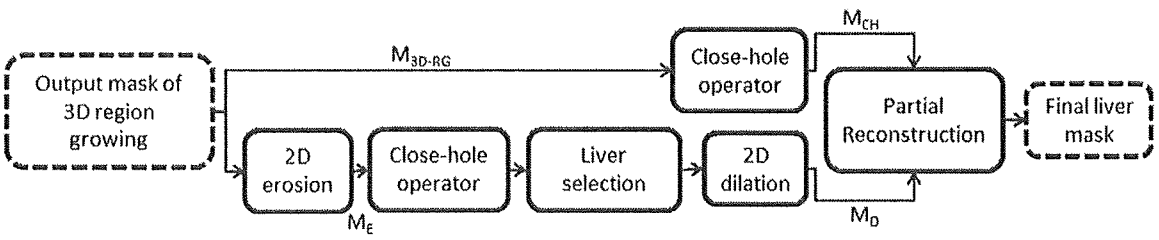

Fig. 4. Post-processing flowchart.

the algorithm. Other 10 dataset were provided (without manual reference) in order to submit the obtained masks and then, an independent observer evaluates the liver segmentation method with five coefficients and a score system.[2] This approach ensures the validity and independence of the final results. The size of each slice was 512×512 pixels. The number of slices of each volume varied from 64 to 348, depending on the dataset. Pixel spacing was between 0.55 and 0.88 mm in x/y direction and slice distance was between 1 and 3 mm.[2]

In the sliver07 dataset, the five coefficients used to obtain the goodness of the method have been: Volumetric Overlap Error (VOE) or Jaccard Coefficient (JC), Relative Volume Difference (RVD), Average Symmetric Surface Distance (ASSD), Root Mean Square Symmetric Surface Distance (RMSD) and Maximum Symmetric Surface Distance or Hausdorff Distance (HD).[2]

The parameters to be tuned in our method are the structuring element of the 2D erosion (and 2D dilation), $B_1(x)$, and the number of iterations in the partial reconstruction, N, both used in the post-processing stage. After different tests with the 20 training sliver07 datasets, the best results were achieved for a circular $B_1(x)$ of radius 5 and $N = 3$.

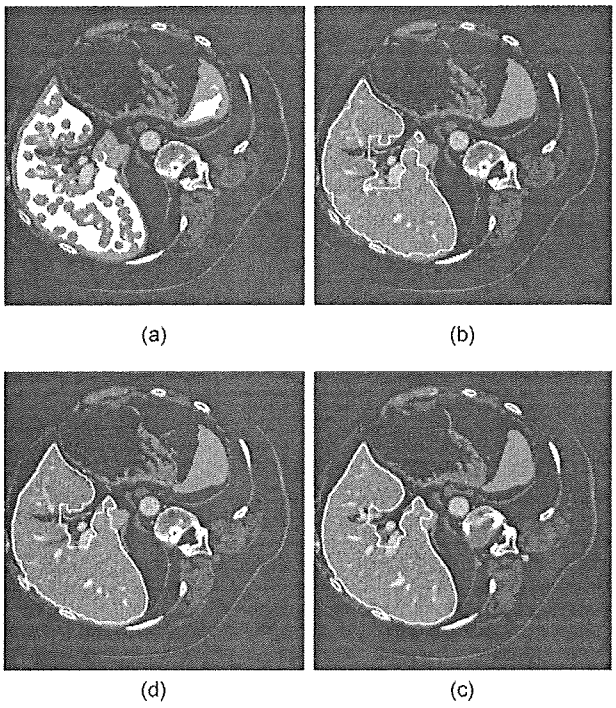

Fig. 5. Liver masks superimposed to original image resulting to algorithm steps (a) 2D eroded mask; (b) dilated contour; (c) contour after partial reconstruction; (d) final contour.

Table I shows the average (m_{test}) and the standard deviation (σ_{test}) of the five coefficients of the 10 test studies evaluated by an independent observer and the average (m_{train}) and the standard deviation (σ_{train}) of the five coefficients of the 20 training studies whose manual reference is open access.[2,24] Additionally, the Dice Coefficient (DC) has been also computed for comparison purposes.

All the results were calculated on an Intel core i5 @ 2.80 GHz, with a RAM of 2 GHz and Windows 7 (32 bits). The runtime average of the 30 datasets (20 training and 10 test) is 0.25 seconds per slice. A typical study, 120–140 slices, is processed in 30–35 seconds.

Additionally, Figures 6 and 7 show respectively the results of different steps of the algorithm and 3D liver results of a private dataset. These CT studies are provided by the "Hospital Universitario y Politécnico La Fe de Valencia" but a manual segmentation is not available and therefore, quantitative coefficients can't be computed. These images are acquired in Toshiba Aquilion and Philips Brilliance CT machines and image resolution and spacing have not significant differences with the sliver07 dataset. This dataset contains healthy and unhealthy patients and the sequence used for the segmentation of the liver is the portal phase because in this sequence the liver appears better contrasted than in others. The qualitative results are very similar to the public studies shown in Table I and are depicted in Figures 3 and 5. The parameters used for these private CT studies are the same that in the sliver07 dataset, which demonstrates the good performance of the method in different situations and that is not needed new parameter settings to work properly with different input conditions.

3.1. Influence of the Noise Reduction Filter

The influence of the noise reduction (or smoothing) filter was calculated by applying different smoothing filters and obtaining the five coefficients in the 20 training datasets. Table II shows the average of the most representative coefficients for the different filters applied in the pre-processing step.

3.2. Influence of User-Iteration in the Seed Selection

To evaluate the dependence of the algorithm accuracy with the seed selection, a final test was carried out. The selected seed

Table I. Final results of the 20 training dataset.

	VOE/JC (%)/(0–1)	RVD (%)	ASSD (mm.)	RSMD (mm.)	HD (mm.)	DC (0–1)
m_{test}	8.78/0.91	−4.83	1.49	3.2	26.68	0.95
(σ_{test})	(2.78)/(0.03)	(2.21)	(0.72)	(1.84)	(10.42)	(0.02)
m_{train}	8.48/0.92	−3.68	1.62	3.65	31.83	0.96
(σ_{train})	(1.67)/(0.02)	(2.83)	(0.62)	(1.57)	(10.7)	(0.01)

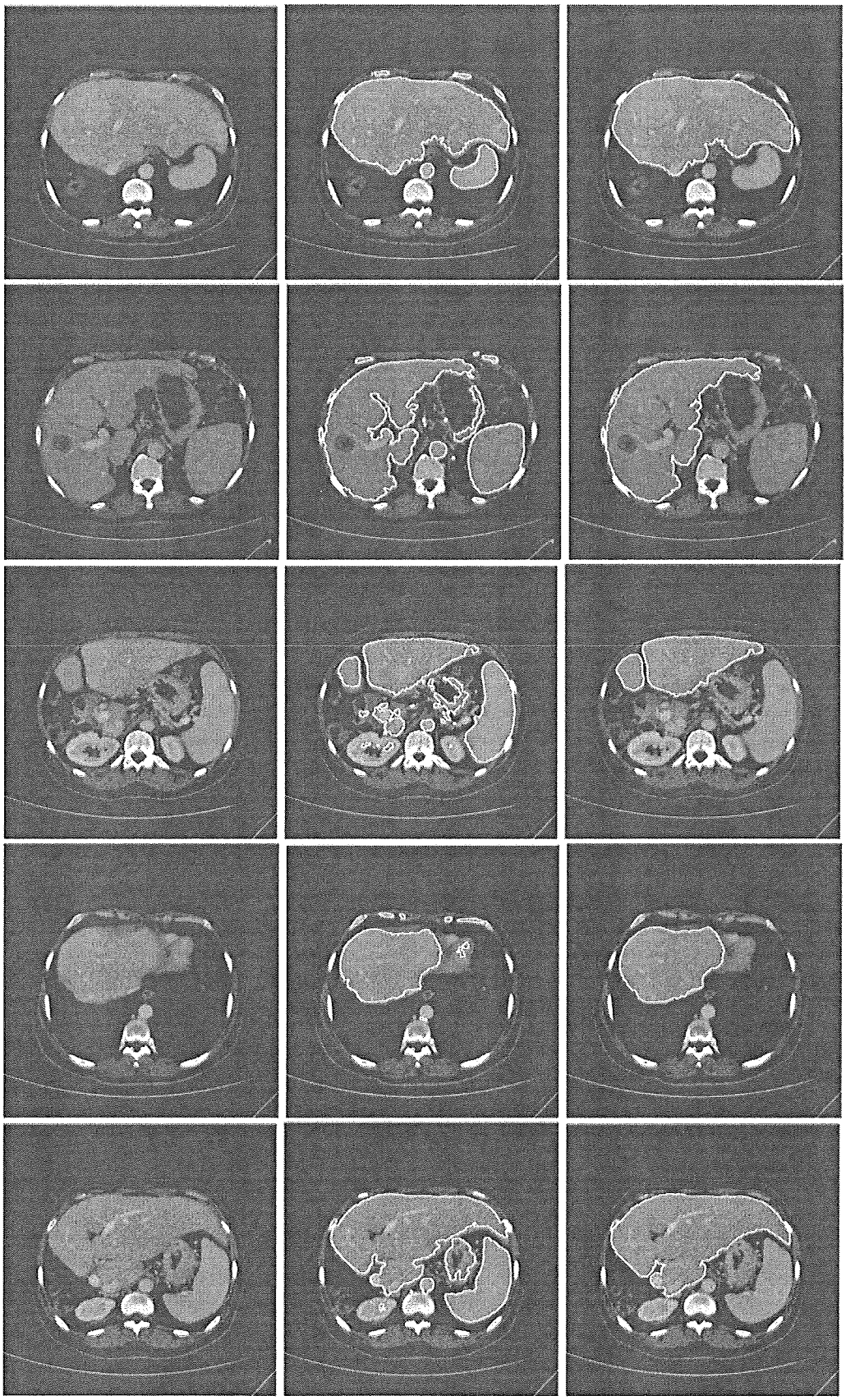

Fig. 6. Liver masks overlayed on the original image resulting to algorithm steps. (a) Original image; (b) after 2D erosion; (c) final contour.

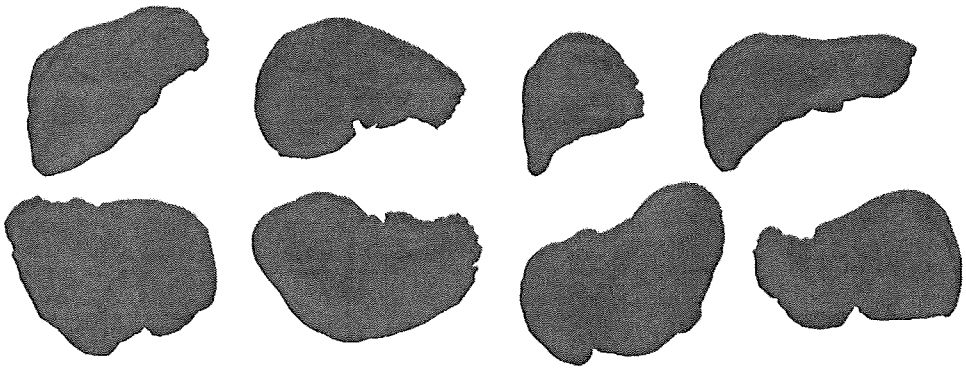

Fig. 7. 3D Liver models of the private dataset.

by one expert in one dataset was stored (called from now the expert seed). Ten random seeds were generated. The restrictions to select the random seeds were to have a similar greylevel (between ± standard deviation in a circular neighbourhood of radius 25 pixels) to the seed selected by the expert and to be in a position relative close (a sphere of radius 5 cm was selected) to the expert seed. This procedure tried to emulate the seed selection by a new user who will probably select the seed in a slice where the liver appears as large as possible and with homogenous level intensity (in a region with similar greylevel and not inside a vessel or in a caudal or cranial slice). The algorithm was run ten times using one of the ten random seeds each time and the average and the standard deviation of the most representative coefficients can be observed in Table III. The first row shows the results using the expert seed (previously included in the Table II). The dataset selected for this experiment was the one that got the closest coefficients to the coefficient average of the twenty training datasets.

4. DISCUSSION

Table IV provides the most promising results and features of methods presented in the state of the art for comparison purposes. It has been demonstrated that the Jaccard Coefficient and the Hausdorff Distance are the most significant coefficients for volume comparison,[29] so these two coefficients (and the dice coefficient for comparative purposes) and the computational cost are provided. The authors[5, 8, 10, 13, 14] use the same sliver07 dataset (10 test studies) than in this work, so the results are directly comparable. The last 5 authors of this Table IV[7, 9, 11, 12, 16] use not publicly available datasets and the comparison is not direct. It is observable that methods with better accuracy than ours required a high user interaction[8, 10] or a high computational cost.[5, 7, 9, 12–14] In Refs. [12, 16] no user interaction or training is required but accuracy is lower than our method[16] or computational cost is higher.[12] These methods[12, 16] use the region growing method in some part of the whole process of the liver segmentation, so it is demonstrated the benefits that this algorithm can produce in our purpose.

In Ref. [2], several authors published their methods and results in the same ten test datasets (whose manual segmentation is not published). These methods are divided in automatic and interactive methods for comparison purpose. To compare our algorithm with interactive methods it is important to specify that these methods require a hard initialization in comparison to our method. In most cases an initial contour has to be provided for initialization purpose or several seeds located in specific zones of the liver. Additionally, these methods require a computational cost between 7 and 60 minutes per dataset. These features make these methods accuracy higher than ours (a VOE less than 7% in most cases) but they reduce considerably the clinical usability of these methods in comparison to ours.

If the ten automatic methods published in Ref. [2] are analysed, the accuracy is lower than the one obtained by interactive methods and only two of them[13, 14] have a VOE lower than our method (other coefficients have similar tendency). However, these two methods need more than 115 and 35 training datasets, respectively, and they require 7 and 15 minutes, respectively, for the segmentation of one patient, in any case higher than our method.

Finally, other region growing algorithms have been analysed and compared with our approach. In Ref. [2] an interactive method and an automatic method are based on this algorithm. In both cases, they produce lower accuracy and higher computational cost than our method. In Ref. [17], a 2D region growing method is applied to liver segmentation and a runtime of 3.53 seconds per slice is obtained, but quantitative results are not provided. Finally, in Ref. [16] a sophisticated 3D region growing algorithm is applied on CT images in venous phase and the results in the 20 training datasets that we use in our work are provided. The same five coefficients are computed; the VOE is 8.2% (in our training datasets is similar, 8.48%) but the standard deviation (±4.1) is higher than our method (±1.67) so the variability and the robustness of our method is higher.

Table II. Results with different noise reduction filters.

Smooth. filter	VOE (%)	HD (mm.)
Morphological center	11.37	32.23
Curvature flow filter	10.24	32.85
Adaptive filter (our proposal)	8.47	31.83

Table III. Results obtained with the expert seed and the average and standard deviation of the results obtained with the random seeds.

Seeds	VOE (%)	HD (mm.)
Radiol. seed	8.47	24.41
m_{10} □$_{10}$□	8.44	21.97
	(0.77)	(1.33)

Table IV. Accuracy and computational cost of different liver segmentation methods.

Method	VOE (%)	HD (mm)	DC (0–1)	Computational cost	Algorithm features
Our method	**8.78**	**26.68**	**0.95**	**25–30 s**	**1 seed**
Ji et al.[4]	8.3	29.3		35 min	
Yang et al.[7]	5.7	20.02		2 min	≈ 30 seeds in specific positions
Peng et al.[9]	5.5	18.6			High user interaction: initial contour in heart portal vein and liver is needed
Heimann et al.[12]	7.7	30.1		7 min	Training required
Kainmuller et al.[13]	6.6	23.05		15 min	Training required with manual segmentation
Rusko et al.[15]	11.44	28.12		25 s	
Wang et al.[6]		21.49/7.68		18/10 min	Training required with manual segmentation
Casciaro et al.[8]			0.96/0.95	≈ 18 min	
Ciecholewski et al.[10]			0.81		Only for healthy patients
Campadelli et al.[11]			0.95	50 s	Image resolution 256×256

For these reasons, we can conclude that our approach fulfills the requirements needed for clinical practice. It has a high accuracy (in the same order than the best automatic methods with which it has been compared) and a lower variability, which makes it a robust solution. Besides that, the proposed method has a high usability in comparison with others, measured in terms of computational cost and user interaction.

5. CONCLUSIONS AND FUTURE WORK

A liver segmentation method in CT venous phase images is presented in this paper. A 3D region growing algorithm has been evaluated with promising results. The selection of this method is based on easy user interaction, automation (only a seed point introduced by the user is needed), and low computational cost. These are typical requirements in a medical environment. A preprocessing filter to reduce noise is applied due to intrinsic CT images properties. An adaptive filter based on statistical parameters is proposed in this paper and it is compared with other filtering approaches obtaining the best results (Table II). After, a post-processing step is carried out to refine the final results. An averaged VOE coefficient of $8.78\% \pm 2.78$ (or Jaccard index of 0.91 ± 0.03) and a Hausdorff Distance of 26.68 ± 10.42 mm. in the test datasets sliver07 demonstrate that results are promising above all if the high level of automation of the method and the low computational cost is taken into account. The computational cost is about 0.25 seconds per slice, in a typical study of 120 slices, the software needs 30 seconds for obtaining the 3D final mask. The user interaction is only related to a seed selection, the other parameters were tuned with the training datasets. For this reason, the variability of this seed selection has been measured (Table III) and the low coefficients variability state user independence of the algorithm.

Regarding future work lines, new approaches of our method will be focused on applying some variation of the watershed transform, like the marker-controlled paradigm[30] or the stochastic watershed[31] in order to improve the accuracy in some areas of the actual region growing method presented in this work. Watershed algorithm does not increase considerably the computational cost and it has easy user interaction. The problem of watershed transform is the initial separation between foreground and background which is equivalent to compute regional minima in the gradient of the image and therefore, an over-segmentation may appear in the original transform. To define these minima and reduce the over-segmentation problem, the final mask obtained with the approach presented in this paper could be used to obtain the needed internal markers in order to apply a 3D marker controlled algorithm for improving the accuracy of our method and for segmenting other areas that are currently not accurately segmented.

Acknowledgments: Thanks to the Hospital Clínica Benidorm (HCB) for funding this project. This work has been supported by the Centro para el Desarrollo Tecnológico Industrial (CDTI) under the project ONCOTIC (IDI-20101153), partially by the Ministry of Education and Science Spain (TIN2010-20999-C04-01).

References and Notes

1. C. Li, X. Wang, S. Eberl, M. Fulham, Y. Yong, C. Jinhu, and D. D. Feng, A likelihood and local constraint level let model for liver tumor segmentation from CT volumes. *IEEE Trans. Biomedical Engineering* 60, 2967 **(2013)**.
2. T. Heimann, B. van Ginneken, M. A. Styner, Y. Arzhaeva, V. Aurich, C. Bauer, A. Beck, C. Becker, R. Beichel, G. Bekes, F. Bello, G. Binnig, H. Bischof, A. Bornik, P. M. M. Cashman, Y. Chi, A. Córdova, B. M. Dawant, M. Fidrich, J. D. Furst, D. Furukawa, L. Grenacher, J. Hornegger, D. Kainmüller, R. I. Kitney, H. Kobatake, H. Lamecker, T. Lange, J. Lee, B. Lennon, R. Li, S. Li, H. Meinzer, G. Németh, D. S. Raicu, A. Rau, E. M. van Rikxoort, M. Rousson, L. Ruskó, K. A. Saddi, G. Schmidt, D. Seghers, A. Shimizu, P. Slagmolen, E. Sorantin, G. Soza, R. Susomboon, J. M. Waite, A. Wimmer, and I. Wolf, Comparison and evaluation of methods for liver segmentation from CT datasets. *IEEE Trans. Med. Imag.* 28, 1251 **(2009)**.
3. A. Mharib, A. Ramli, S. Mashohor, and R. Mahmood, Survey on liver CT image segmentation methods. *Artif. Intell. Rev.* 37, 83 **(2011)**.
4. R. Punia and S. Singh, Review on machine learning techniques for automatic segmentation of liver images. *International Journal of Advanced Research in Computer Science and Software Engineering* 3, 666 **(2013)**.
5. H. Ji, J. He, X. Yang, R. Deklerck, and J. Cornelis, ACM-based automatic liver segmentation from 3-D CT images by combining multiple atlases and improved mean-shift techniques. *IEEE Journal of Biomedical and Health Informatics* 17, 690 **(2013)**.
6. H. Park, P. Peyton, H. Bland, and C. R. Meyer, Construction of an abdominal probabilistic atlas and its application in segmentation. *IEEE Trans. Med. Imag.* 22, 483 **(2003)**.
7. G. Wang, S. Zhang, F. Li, and L. Gu, A new segmentation framework based on sparse shape composition in liver surgery planning system. *Medical Physics* 40, 1 **(2013)**.
8. X. Yang, H. C. Yu, Y. Choi, W. Lee, B. Wang, J. Yang, H. Hwang, J. H. Kim, J. Song, B. H. Cho, and H. You, A hybrid semi-automatic method for liver segmentation based on level-set methods using multiple seed points. *Computer Methods and Programs in Biomedicine* 113, 69 **(2014)**.
9. S. Casciaro, R. Franchini, L. Massoptier, E. Casciaro, F. Conversano, A. Malvasi, and A. Lay-Ekuakille, Fully automatic segmentations of liver and hepatic tumors from 3-D computed tomography abdominal images: Comparative evaluation of two automatic methods. *IEEE Sensors Journal* 12, 464 **(2012)**.
10. J. Peng, Y. Wang, and D. Kong, Liver segmentation with constrained convex variational model. *Pattern Recognition Letters* 43, 81 **(2014)**.
11. M. Ciecholewski, Automatic liver segmentation from 2D CT images using an approximate contour model. *Journal of Signal Processing Systems* 74, 151 **(2013)**.

12. P. Campadelli, E. Casiraghi, and A. Esposito, Liver segmentation from computed tomography scans: A survey and a new algorithm. *Art. Int. Med.* 45, 185 **(2009)**.
13. T. Heimann, H.-P. Meinzer, and I. Wolf, A statistical deformable model for the segmentation of liver CT volumes, *Proc. MICCAI Workshop 3-D Segmentation Clinic: A Grand Challenge*, Brisbane **(2007)**, pp. 161–166.
14. D. Kainmuller, T. Lange, and H. Lamecker, Shape constrained automatic segmentation of the liver based on a heuristic intensity model, *Proc. MICCAI Workshop 3-D Segmentation Clinic: A Grand Challenge*, Brisbane **(2007)**, pp. 109–116.
15. L. Haibin, S. K. Zhou, Y. Zheng, B. Georgescu, M. Suehling, and D. Comaniciu, Hierarchical, learning-based automatic liver segmentation, *Proc. IEEE Conference on Computer Vision and Pattern Recognition*, Anchorage **(2008)**, pp. 1–8.
16. L. Ruskó, G. Bekes, and M. Fidrich, Automatic segmentation of the liver from multi- and single-phase contrast-enhanced CT images. *Med. Image Anal.* 13, 871 **(2009)**.
17. Y. Chen, Z. Wang, W. Zhao, and X. Yang, Liver segmentation from CT images based on region growing method, *3rd International Conference on Bioinformatics and Biomedical Engineering*, Beijing **(2009)**, pp. 1–4.
18. L. Soler, H. Delingette, G. Malandain, J. Montagnat, N. Ayache, C. Koehl, O. Dourthe, B. Malassagne, M. Smith, D. Mutter, and J. Marescaux, Fully automatic anatomical, pathological, and functional segmentation from CT scans for hepatic surgery. *Computer Aided Surgery Official Journal of the International Society for Computer Aided Surgery* 6, 131 **(2001)**.
19. O. Gloger, J. Kühn, A. Stanski, H. Völzke, and R. Puls, A fully automatic three-step liver segmentation method on LDA-based probability maps for multiple contrast MR images. *Magn. Reson. Imaging* 28, 882 **(2010)**.
20. S. Milko, E. Samset, and T. Kadir, Segmentation of the liver in ultrasound: A dynamic texture approach. *International Journal of Computer Assisted Radiology and Surgery* 3, 143 **(2008)**.
21. C.-Y. Hsu, C.-Y. Liu, and C.-M. Chen, Automatic segmentation of liver PET images. *Computerized Medical Imaging and Graphics* 32, 601 **(2008)**.
22. C. Li, X. Wang, Y. Xia, S. Eberl, Y. Yin, and D. D. Feng, Automated PET-guided liver segmentation from low-contrast CT volumes using probabilistic atlas. *Computer Methods and Programs in Biomedicine* 107, 164 **(2012)**.
23. HepaPlan Project, www.labhuman.com, Access April **(2013)**.
24. Liver Segmentation Challenge, http://sliver07.org/results.php, Access April **(2013)**.
25. J. Serra, Image Analysis and Mathematical Morphology, Academic Press, Orlando **(1982)**, Vol. I.
26. P. Soille, Morphological Image Analysis, 2nd edn., Springer, Germany **(2002)**.
27. L. Ibañez, W. Schroeder, L. Ng, and J. Cates, The insight software consortium, The ITK Sotware Guide, 2nd edn., Kitware Inc. **(2005)**.
28. C. T. Zahn and R. Z. Roskies, Fourier descriptors for plane closed curves. *IEEE Trans. Comp.* c-21, 269 **(1972)**.
29. M. A. Lago, F. Martínez-Martínez, M. J. Rupérez, C. Monserrat, and M. Alcañiz, A study about coefficients to estimate the error in biomechanical models used to virtually simulate the organ behaviors. *Studies in Health Technology and Informatics* 173, 250 **(2012)**.
30. F. Meyer and S. Beucher, Morphological segmentation. *Journal of Visual Communication and Image Representation* 1, 21 **(1990)**.
31. J. Angulo and D. Jeulin, Stochastic watershed segmentation, *Proc. of the 8th International Symposium on Mathematical Morphology*, Rio de Janeiro **(2007)**, pp. 265–276.

Received: 14 July 2014. Revised/Accepted: 13 December 2014.